

KHAN, L.U., YOUNAS, M., KHAN, S.U. and REHMAN, M.Z.U. 2020. Synthesis and characterization of CoFe₂O₄/MWCNTs nanocomposites and high-frequency analysis of their dielectric properties. *Journal of material engineering and performance* [online], 29(1), pages 251-258. Available from: <https://doi.org/10.1007/s11665-020-04572-9>

Synthesis and characterization of CoFe₂O₄/MWCNTs nanocomposites and high-frequency analysis of their dielectric properties.

KHAN, L.U., YOUNAS, M., KHAN, S.U. and REHMAN, M.Z.U.

2020

This version of the article has been accepted for publication, after peer review (when applicable) and is subject to Springer Nature's [AM terms of use](#), but is not the Version of Record and does not reflect post-acceptance improvements, or any corrections. The Version of Record is available online at: <https://doi.org/10.1007/s11665-020-04572-9>

Synthesis and Characterization of CoFe₂O₄/MWCNTs Nanocomposites and High-Frequency Analysis of their Dielectric Properties

Latif Ullah Khan^{1†}, Muhammad Younas², Shafi Ullah Khan³, Zia Ur Rehaman²

¹ School of Chemical and Materials Engineering, National University of Sciences and Technology, Islamabad, 44000, Pakistan.

² School of Mechanical and Manufacturing Engineering, National University of Sciences and Technology, Islamabad, 44000, Pakistan.

³ Department of Chemical Engineering, University of Engineering and Technology, Peshawar, Pakistan.

†Corresponding author:

Latif Ullah Khan

Current Address: School of Chemical and Materials Engineering (SMME), National University of Sciences and Technology (NUST), Sector H-12, Islamabad 44000, Pakistan.

Email Address: latif_mse10@scme.nust.edu.pk

Abstract

Nanoparticles of CoFe₂O₄ were synthesized by chemical co-precipitation method. While, CoFe₂O₄/MWCNTs nanocomposites were synthesized with increasing contents of MWCNTs i.e. 0.0%, 2.0%, 3.0% and 5.0% by weight via ultrasonication method in a dispersive medium using ortho-xylene. The synthesized cobalt ferrite nanoparticles and their nanocomposites were characterized by Impedance Analyzer, Fourier Transform Infrared Spectroscopy (FTIR), Scanning Electron Microscope (SEM), and X-ray diffraction (XRD) techniques. The XRD indexed patterns confirmed the face-centered cubic structure of CoFe₂O₄/MWCNTs nanocomposites. The average crystallite size in all the samples was in the range of 15 to 35 nm. The decorations of CoFe₂O₄ on MWCNTs were confirmed by SEM images. The FTIR results showed two vibrational bands. With the increasing contents of multi-walled carbon nanotubes in the cobalt ferrite/MWCNTs nanocomposites, the dielectric properties were also enhanced. At 1 MHz, dielectric constant, dielectric loss and tangent loss factor were increased from 26, 15.1, 0.580 for pure cobalt ferrite to 47, 28.9, 0.614 for loading of 5% MWCNTs respectively. While at 1GHz, dielectric constant, dielectric loss and tangent loss factor were increased from 11.6, 0.33, 0.028 for pure cobalt ferrite to 19.4, 0.61, 0.031 for loading of 5% MWCNTs respectively.

Such huge increase in the dielectric properties of cobalt ferrite and multi-walled carbon nanocomposites exploited their applications at high frequency.

Keywords:

Co-precipitation, Scanning Electron Microscope (SEM), Impedance Analyzer, X-ray Diffraction (XRD), Fourier Transform Infrared Spectroscopy (FTIR), Nanocomposites.

1. Introduction

Due to the massive usage of high-carbon energy, environmental degradation, and energy crisis are continuously increasing. In recent scientific research, the need to discover low-carbon and sustainable sources of energy are seeking attention worldwide [1, 2]. Ferrites generally represented by MFe_2O_4 (M= Ni, Co, Zn, Mn, etc.) called spinel ferrites that exhibits cubic spinel structure has shown improved optical, magnetic and electrical properties [3]. Spinel ferrites have been extensively studied due to their applications in supercapacitors, microwave devices, high-density magnetic recording, magnetic fluids, and medical diagnostics [4-7]. In this research work, $CoFe_2O_4$ was synthesized via chemical co-precipitation method. Although nanoparticles of spinel ferrites can be prepared by numerous methods such as sol-gel techniques [8], solvothermal [9, 10], co-precipitation [11], hydrothermal synthesis [12], mechanical alloying [13], auto-combustion [14, 15] and microemulsion method [16, 17].

Owing to the high aspect ratio of the carbon nanotubes (CNTs), it attracts worldwide attention having an sp^2 hybridized structure with multiple layers of graphene rolled over one another [2, 18]. CNTs may be classified into three types namely, multi-walled carbon nanotubes (MWCNTs), single-walled carbon nanotubes (SWCNTs) and junctions-crosslinking. In recent years, researchers have paid special attention to MWCNTs due to their exceptional physical, chemical [19, 20] and electrical [21] properties, huge surface area, high aspect ratio, and nanosized stability which shows their capability in the field of nanoscience engineering.

MWCNTs coupled with nanoparticles of ferrites can be widely used in magnetic force microscopy, drug delivery [9], purification of water [22], dielectrics [23-26] and removal of uranium from aqueous solution [27], etc. In order to optimize the potential abilities of the ferrite's nanoparticles, various techniques are used for the decoration of nanoparticles over MWCNTs. Due to their huge dielectric losses, these nanohybrids are preferred for EMI shielding, dielectric and microwave absorption properties [28, 29]. At room temperature, researchers have noticed the ferromagnetic behavior of ferrites/MWCNTs nanohybrids [30]. It has also been reported that due to enhanced microwave absorption properties, CNTs/ferrites

nanohybrids have significant utilization for reflection losses in military applications [22]. The real and imaginary part of permittivity also enhances by the introduction of CNTs which permit their application at high frequencies [28]. In this research work, the synthesized cobalt ferrite/MWCNTs nanocomposites were studied and confirmed by utilizing FTIR, XRD, SEM and Impedance Analyzer. Finally, the high frequency dielectric nature of $\text{CoFe}_2\text{O}_4/\text{MWCNTs}$ (MWCNTs=0.0%, 2.0%, 3.0%, 5.0%) system was analyzed at room temperature.

2. Materials and Synthesis Procedure

2.1 Materials

Chemicals used in the synthesis include; $\text{Fe}(\text{NO}_3)_3 \cdot 9\text{H}_2\text{O}$ supplied by EMSURE® Merck KGaA Darmstadt Germany (99.5% purity), $\text{Co}(\text{NO}_3)_2 \cdot 6\text{H}_2\text{O}$ supplied by Scharlau, Scharlab S.L Spain (99% purity), NaOH supplied by Fischer Chemical Ltd. – Hong Kong (99% purity) and ortho-xylene (99% purity) and MWCNTs (99% purity) supplied by Sigma Aldrich. All these reagent grade chemicals were utilized without any additional decontamination. Deionized and double distilled water was utilized for the synthesis of cobalt ferrite nanoparticles as a solvent and for washing purposes respectively.

2.2 Synthesis Procedure

0.1 M solution of $\text{Co}(\text{NO}_3)_2 \cdot 6\text{H}_2\text{O}$ and 0.2 M solution of $\text{Fe}(\text{NO}_3)_3 \cdot 9\text{H}_2\text{O}$ were taken in separate glass beakers using deionized water and magnetically stirred it for 10 minutes. In order to make a complete homogenous solution, both the samples were then mixed and magnetically stirred for 25 minutes at room temperature. Then it was placed on a hot plate until temperature of the above-mixed solution reached to 90 °C. 3 M preheated solution of NaOH at 90 °C prepared in a separate beaker and rapidly poured to the cobalt nitrate hexahydrate and iron nitrate (III) nonahydrate solution. The resulting solution was maintained at 90 °C for an hour followed by continuous magnetic stirring, then switched off heating until the temperature reached ambient temperature followed by washing with double distilled water to achieve pH value of 7. Samples were then dried in the oven by maintaining overnight heating at 110 °C to obtain moisture-free desired powders. To obtain discrete spinel phase by eliminating any carbonaceous impurity, these powders were calcinated for eight hours at 820 °C. For synthesizing desired nanocomposites, MWCNTs were dispersed uniformly in a beaker utilizing polar solvent of o-xylene kept in ultra-sonication bath. Similarly, cobalt ferrite nanoparticles were dispersed uniformly in a beaker utilizing o-xylene kept in ultra-sonication bath. Sonicated mixture of cobalt ferrite nanoparticles was then added drop by drop to MWCNTs dispersion and sonicated for 16

hours. For complete drying, it was kept in the oven obtaining porous powders and then mechanically homogenized. For studying the effect of increasing contents of MWCNTs on the dielectric properties of cobalt ferrite, the concentration of MWCNTs was varied for 0.0%, 2.0% (0.03 grams), 3.0% (0.045 grams) and 5.0% (0.075 grams) in each sample respectively. In this research, the E4990A Impedance Analyzer was used to record the dielectric properties of each sample as a function of frequency from 1MHz to 1GHz. X-ray diffraction using CuK α radiation (having wavelength of 1.5405 Å) in the range of 20–80° was utilized for the determination of the crystal structure and phase formation at ambient temperature. The structural morphology was studied by SEM (Model No.6390). The existence of oxygen-metal lattice sites and bonding nature were explored by FTIR spectroscopy (Perkin Elmer spectrum 100) utilizing KBr powder in preparing pellets of cobalt ferrite and cobalt ferrite/MWCNTs nanocomposites. Pellets having diameter 10 mm with varying thicknesses were prepared by applying load up to 4-5 tons using a hydraulic press for dielectric and electric measurements.

3. Results and Discussion

3.1 X-ray Diffraction

Figure 1 indicates the x-ray diffraction patterns of calcined powder of CoFe₂O₄ and CoFe₂O₄/MWCNTs nanocomposites obtained at ambient temperature. Table 2 lists the XRD peaks of (220), (311), (222), (400), (422), (511), (440) and (533) exhibiting Fd-3m space group at 2 θ Braggs angle. The observed peaks were well indexed in conformity with the characteristic's peaks of these materials in JCPDS card No.00–022-1086, validating FFC spinel structure formation. The crystallite size in case of each sample for the most intense peak i.e. (311) was calculated by Debye-Scherrer's equation [31]. The calculated crystallite sizes were listed in Table 1. No other peaks of MWCNTs were observed in cobalt ferrite's nanocomposites, representing their synthesis route efficiency. A small sharp peak may be observed at 26° when the weight percentage of MWCNT exceeds 7 %.

Porosity fraction plotted against MWCNT's contents is shown in Figure 2. Bulk density and x-ray density plotted against multi-walled carbon nanotubes contents are shown in Figure 3. The various values of porosity, bulk density and x-ray density against multi-walled carbon nanotubes contents (wt. %) are listed in Table 1 and calculated using Equation (1), (2) and (3).

$$Porosity\ Fraction = 1 - \left(\frac{Bulk\ Density}{Xray\ Density} \right) \quad (1)$$

$$\text{Bulk Density} \left(\frac{g}{cm^3} \right) = \frac{\text{mass(Pellet's Mass in grams)}}{\text{volume(Pellet's Volume in } cm^3)} \quad (2)$$

$$\text{Xray Density} \left(\frac{g}{cm^3} \right) = \frac{\text{Number of Atoms per Unit Cell} \times \text{Molecular Mass}}{\text{Volume of Unit Cell} \times \text{Avagadro's Number}} \quad (3)$$

Due to lots of heptagon-pentagon pair defects and interstitials observed in MWCNTs are confirming their porous nature [32]. That's why MWCNTs have higher volume with low mass. Bulk density was calculated by division of mass of the prepared pellets of cobalt ferrite and its nanocomposite with MWCNTs by volume of pellets and was plotted against MWCNTs contents which show the decreasing trend with increasing contents of MWCNTs. The decreasing trend was also noticed in the case of x-ray density with increasing contents of MWCNTs. Generally, porosity shows increasing trend with increasing contents of MWCNTs because of MWCNTs porous filler matrix addition, more interfaces are formed that results in producing of large number of voids hence confirming their increasing trend [33].

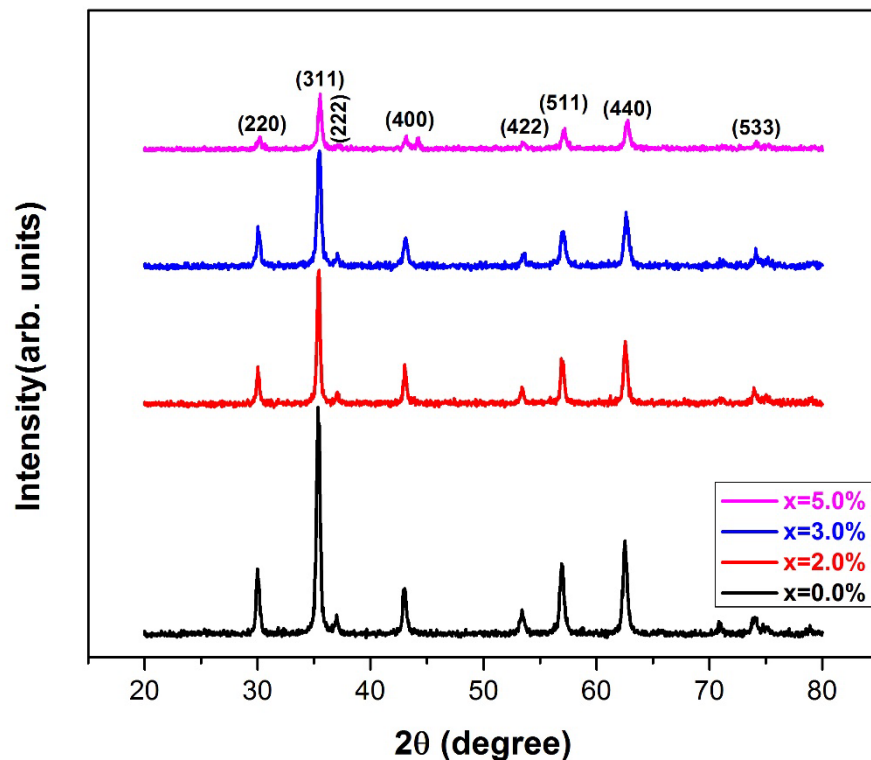


Figure 1: X-ray diffraction patterns of pure CoFe₂O₄ and CoFe₂O₄/MWCNTs nanocomposite.

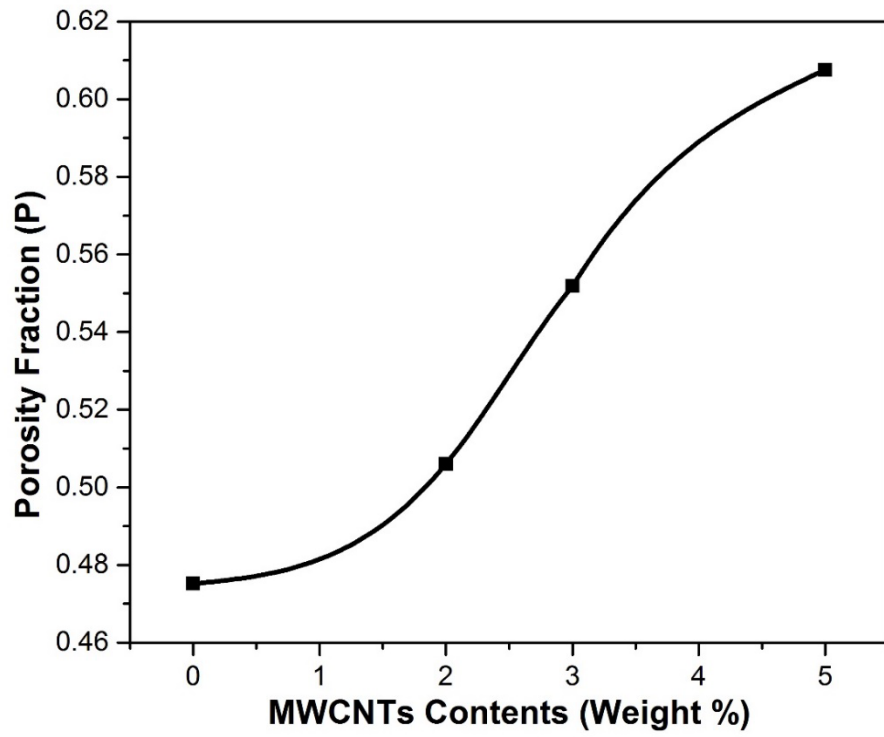


Figure 2: Porosity fraction variation as a function of MWCNTs contents (wt. %) for pure CoFe_2O_4 and $\text{CoFe}_2\text{O}_4/\text{MWCNTs}$ nanocomposite.

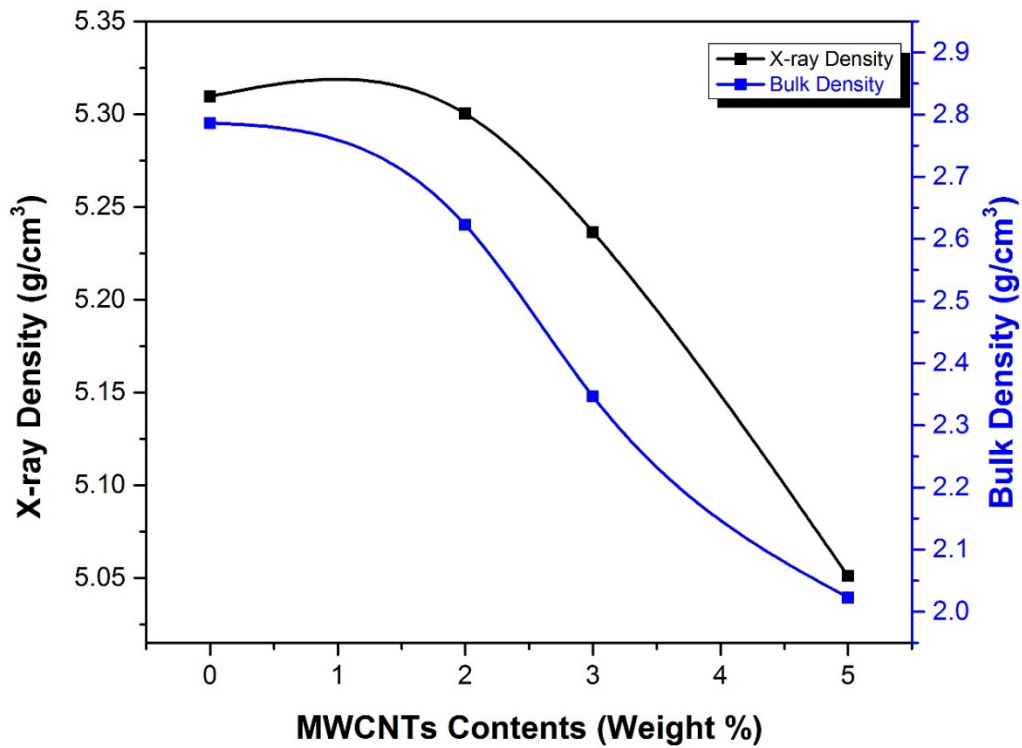


Figure 3: Bulk Density and X-ray Density variations as a function of MWCNTs contents (wt. %) for pure CoFe_2O_4 and $\text{CoFe}_2\text{O}_4/\text{MWCNTs}$ nanocomposite.

Table 1: Variation of crystallite size, porosity, bulk density and x-ray density of pure CoFe_2O_4 and $\text{CoFe}_2\text{O}_4/\text{MWCNTs}$ nanocomposite as a function of MWCNTs contents (wt. %).

MWCNTs Contents (wt.%)	Crystallite Size (nm)	Porosity (%)	Bulk density (g/cm ³)	X-Ray density (g/cm ³)
0%	35	47.516	2.786	5.3095
2%	26	50.601	2.622	5.3093
3%	30	55.186	2.346	5.236
5%	15	60.761	2.026	5.164

Table 2: Pure CoFe_2O_4 and $\text{CoFe}_2\text{O}_4/\text{MWCNTs}$ nanocomposite's peak position as a function of MWCNTs (wt.%) at various 2θ angle.

MWCNTs Contents (wt.%)	2θ at (220)	2θ at (311)	2θ at (222)	2θ at (400)	2θ at (422)	2θ at (511)	2θ at (440)	2θ at (533)
0%	30.191 ^o	35.558 ^o	43.124 ^o	44.208 ^o	53.532 ^o	57.095 ^o	62.706 ^o	74.193 ^o
2%	30.121 ^o	35.558 ^o	37.049 ^o	43.144 ^o	53.560 ^o	56.985 ^o	62.654 ^o	74.177 ^o
3%	30.104 ^o	35.389 ^o	37.066 ^o	43.068 ^o	53.437 ^o	56.966 ^o	62.561 ^o	73.998 ^o
5%	30.115 ^o	35.388 ^o	37.112 ^o	43.135 ^o	53.545 ^o	56.875 ^o	62.549 ^o	73.397 ^o

3.2 FTIR Spectroscopy

The structural formation of synthesized cobalt ferrites and respective ferrite/MWCNTs nanocomposites were investigated by FTIR spectroscopy at room temperature. For the spectroscopic analysis, KBr base pellets of the respective samples were utilized in the range of 350 cm^{-1} to 1000 cm^{-1} . FTIR spectra of all the samples are shown in Figure 4. The FTIR spectra of the samples are almost identical thus confirming the presence of similar chemical bonding. In all these spectra, two lattice vibration bands were observed which consist of metal ion and oxygen ion thus confirming spinel structure formation. These results were in good similarity with the results described by Waldron et al. [34]. Due to the difference in the metal-oxygen bond lengths at tetrahedral (A) site and octahedral (B) site, a slight difference in these vibrational bands was observed. The stretching vibrational bands around 409 cm^{-1} to 413 cm^{-1} confirm the octahedral (B) position due to $\text{Co}^{+2}\text{-O}^{2-}$ bond while stretching vibrational bands around 582 cm^{-1} to 586 cm^{-1} agree to tetrahedral (A) position due to $\text{Fe}^{+3}\text{-O}^{2-}$ bond in pure CoFe_2O_4 and $\text{CoFe}_2\text{O}_4/\text{MWCNTs}$ nanocomposites.

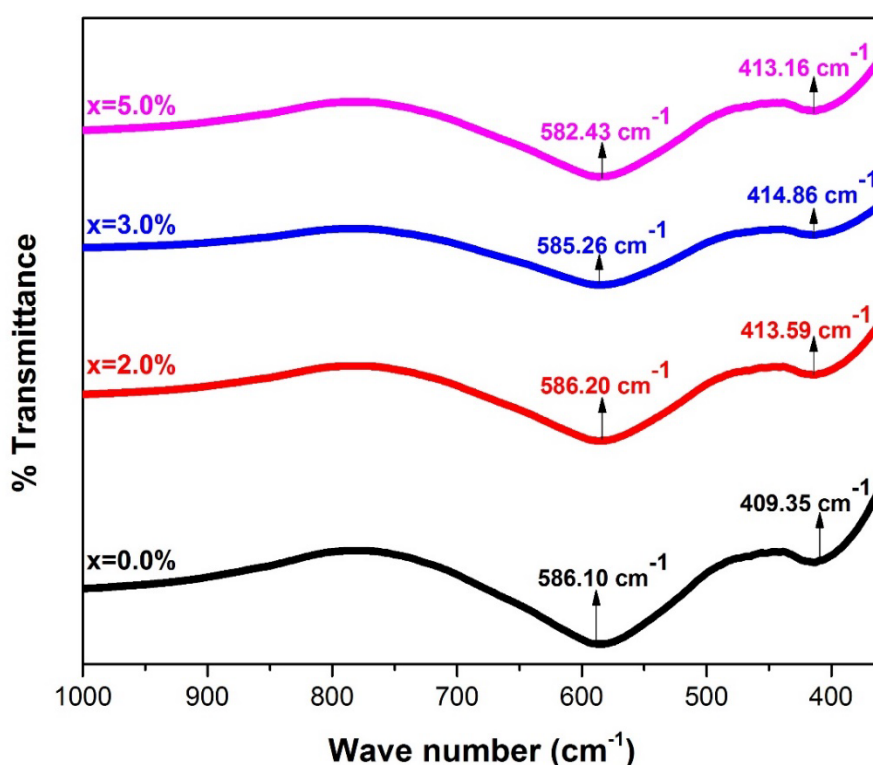


Figure 4: FTIR spectra for $\text{CoFe}_2\text{O}_4/\text{MWCNTs}$ nanocomposite as a function of MWCNT's contents (wt. %).

3.3 Scanning Electron Microscopy

The scanning electron microscope was used to study the surface morphologies of the synthesized pure ferrite and its nanocomposite. The SEM images of surface morphology of CoFe_2O_4 nanoparticles and $\text{CoFe}_2\text{O}_4/\text{MWCNTs}$ nanocomposite for $x=3.0\%$ are shown in Figure 5 and Figure 6 respectively. The SEM image of nanocomposite showed that MWCNTs were decorated uniformly with cobalt ferrite nanoparticles which shows the efficiency of the synthesis method of nanocomposites. The grain size obtained from the SEM is in the range of 23-40 nm. It is also important to mention here that grain size may be present as a single crystal or agglomeration of several crystals. The directional coating of the respective ferrites' nanoparticles was observed on the MWCNTs due to the decrease in surface energy. This decrease in surface energy of the ferrites nanoparticles is due to the o-xylene solvent used in the sonication for long time. Agglomeration can also be seen among ferrites nanoparticles because of their Van Der Waals attraction [35]. Moreover, EDX was also performed for the elemental analysis of CoFe_2O_4 nanoparticles and $\text{CoFe}_2\text{O}_4/\text{MWCNTs}$ nanocomposite. The EDX spectra of the CoFe_2O_4 nanoparticles and $\text{CoFe}_2\text{O}_4/\text{MWCNTs}$ nanocomposite are shown in Figure 7 and Figure 8. The results revealed that the elements Co, Fe, O coexist in the CoFe_2O_4 nanoparticles and Co, Fe, O, C elements coexist in the $\text{CoFe}_2\text{O}_4/\text{MWCNTs}$ nanocomposite. The experimental mass percentage and atomic percentage of CoFe_2O_4 nanoparticles and $\text{CoFe}_2\text{O}_4/\text{MWCNTs}$ nanocomposite are also shown with Figure 7 and Figure 8.

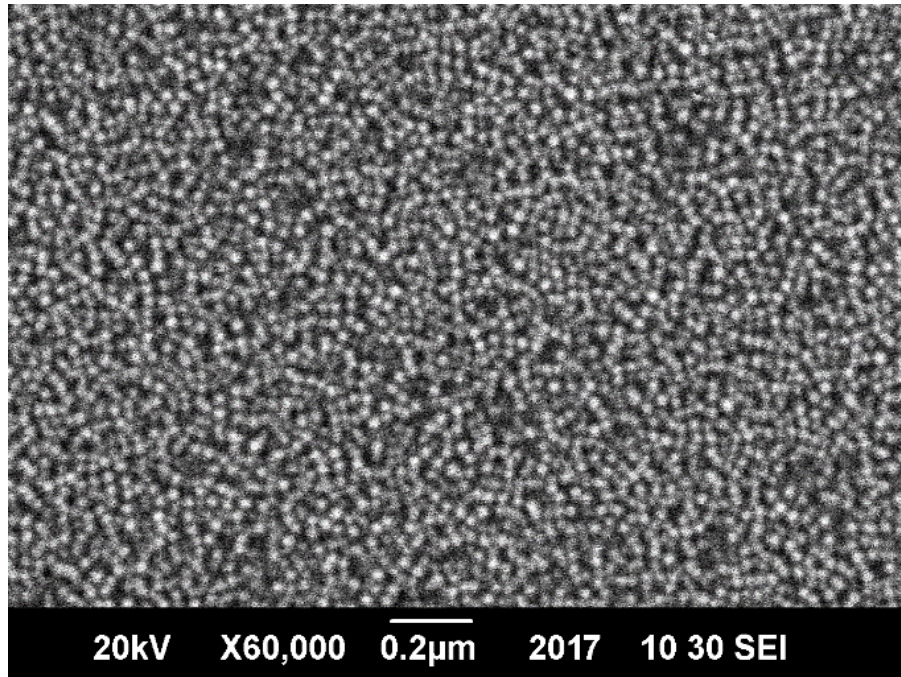


Figure 5: Scanning Electron Microscope image of pure nanoparticles of CoFe_2O_4 .

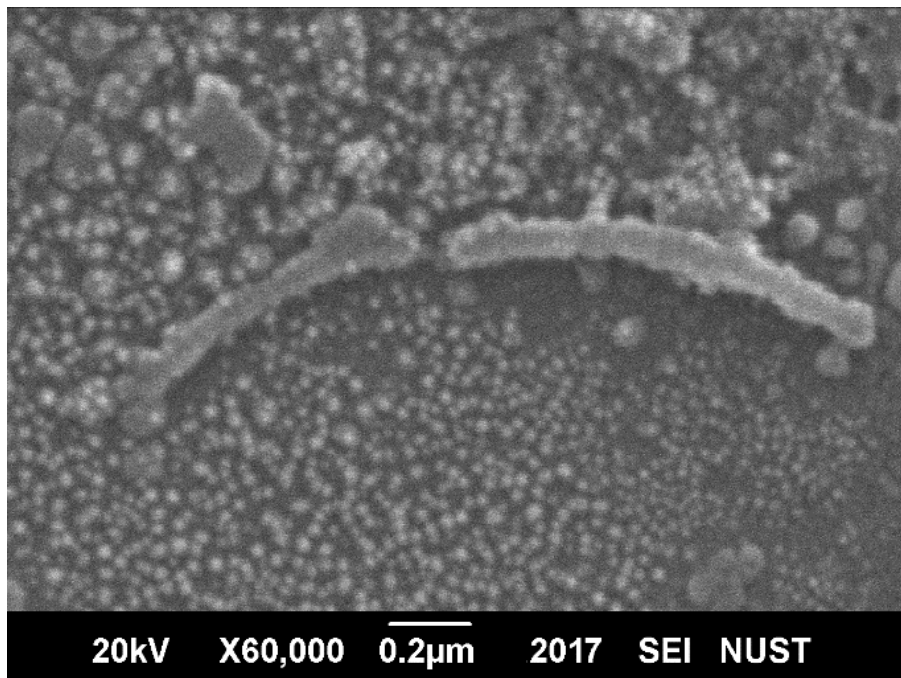


Figure 6: Scanning Electron Microscope image of nanocomposite of CoFe_2O_4 /MWCNTs (x=3.0% MWCNTs).

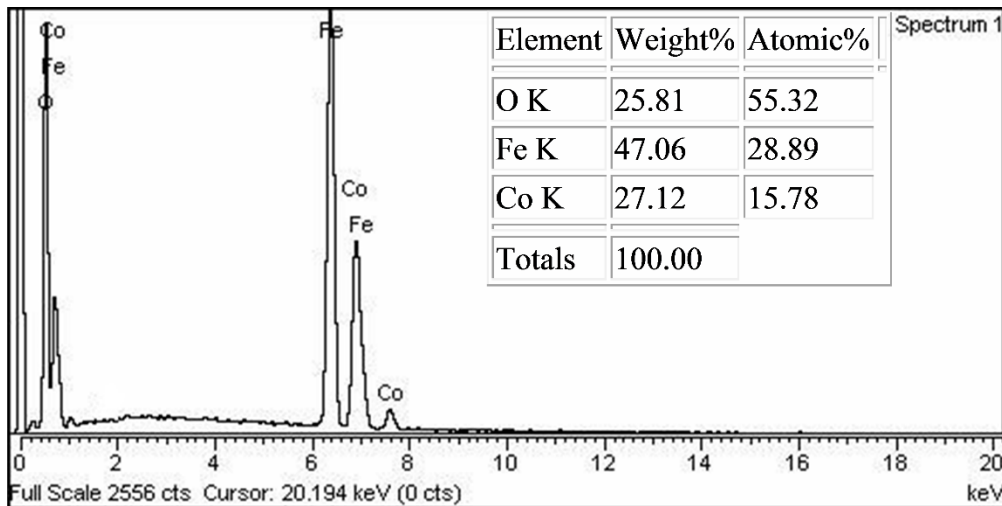


Figure 7: EDX Spectra of CoFe_2O_4 nanoparticles.

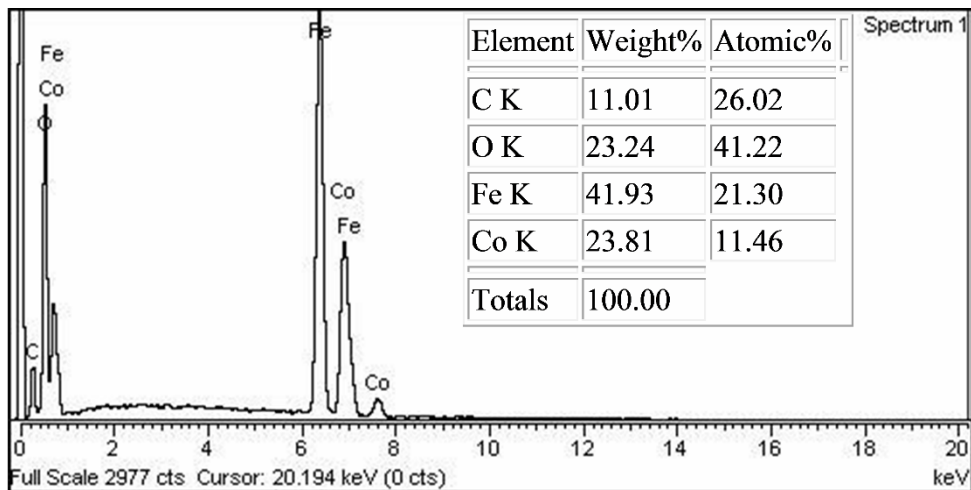


Figure 8: EDX Spectra of $\text{CoFe}_2\text{O}_4/\text{MWCNTs}$ nanocomposite.

3.4 Impedance Analyzer Results

3.4.1 Dielectric Constant

The real part of the permittivity i.e., dielectric constant (ϵ') depends on the operating frequency and is related to the degree of polarization. From the results of dielectric constant, the usage of pure ferrite and respective synthesized nanocomposite for high-frequency applications were investigated. A decreasing trend with the increase in frequency was observed in dielectric constant as shown in Figure 9. This dependence upon frequency of dielectric constant is due the interfacial polarization theory as predicted by Maxwell-Wagner [36]. According to this model, the ferrite's dielectric structure is made up of two layers; a conductive layer that consists of ferrite grains and a high resistive poor conductive layer that consists of grain boundaries. The mechanism through which a polarization in ferrites occurred is similar to the conduction process as indicated by the Novikova and Rabinkin [37]. The local displacement of the electrons occurs in the applied field direction owing to the electron exchange between Fe^{+2} and Fe^{+3} and these electrons determine the polarization.

At low frequency, electrons through hopping mechanism reach the grain boundaries and pile up there owing to highly resistivity i.e., insulative nature of grain boundaries and hence results in polarization. The higher value of dielectric constant at low frequency may also be due to defects, dislocations, and voids, etc. The decrease in dielectric constant with the increasing frequency is because at higher frequency any factors contributing to the polarization are lagging the applied field. The electron hopping cannot follow the applied electric field fluctuations outside a certain frequency boundary causing a decrease in the dielectric constant due to the decrease in interfacial polarization. Table 2 indicated an enormous increase in dielectric constant with increasing contents of MWCNTs. This is because of MWCNTs which are establishing a conductive network in ferrite matrix while acting as a parallel plate capacitor [38]. In ferrite matrix, the polarization contributed by dipole formation boosts the capability of storing charge by enhancing contents of stored charge.

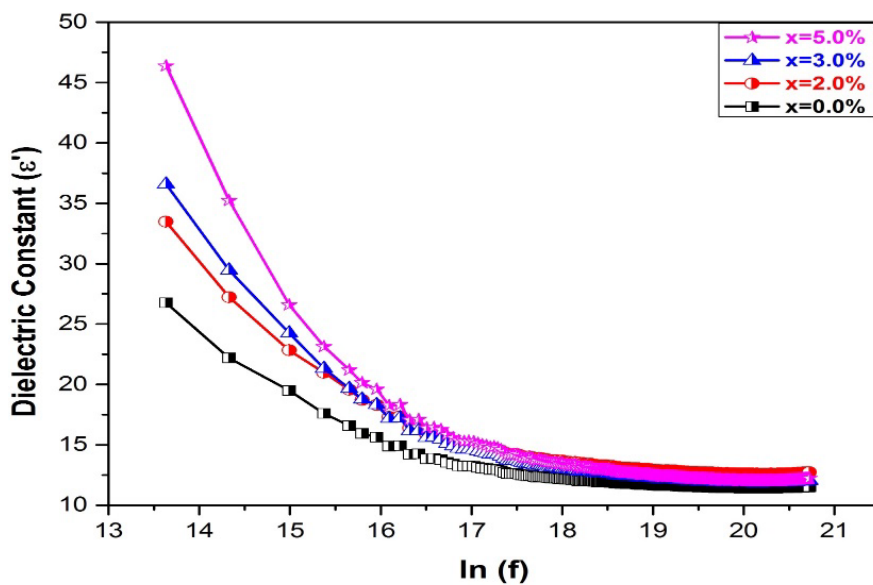


Figure 9: Variation of the dielectric constant of pure CoFe_2O_4 and nanocomposites of $\text{CoFe}_2\text{O}_4/\text{MWCNTs}$ as a function of frequency and MWCNTs contents (wt. %).

Table 3: Variation of dielectric constant (ϵ'), dielectric loss (ϵ''), tangent loss factor ($\tan \delta$) and AC conductivity (σ_{AC}) of the pure ferrite (CoFe_2O_4) and nanocomposites ($\text{CoFe}_2\text{O}_4/\text{MWCNTs}$) as a function of frequency and MWCNTs contents (wt. %).

MWCNTs contents (wt.%)	0.0%	2.0%	3.0%	5.0%
ϵ' (1MHz)	2.6E+01	3.59E+01	4.02E+01	4.70E+01
ϵ' (1GHz)	1.16E+01	1.52E+01	1.69E+01	1.94E+01
ϵ'' (1MHz)	1.51E+01	1.98E+01	2.19E+01	2.89E+01
ϵ'' (1GHz)	3.32E-01	3.85E-01	4.71E-01	6.11E-01
Tan δ (1MHz)	0.580	0.551	0.544	0.614
Tan δ (1GHz)	0.28E-01	0.254E-01	0.280E-01	0.314E-01
σ_{AC} (1MHz)	0.001100	0.001431	0.001709	0.005709
σ_{AC} (1GHz)	0.02139	0.03050	0.1416	0.1456

3.4.2 Dielectric Loss

The imaginary part of permittivity i.e., dielectric loss (ϵ'') is related to the energy dissipation that depends upon operational frequency of pure cobalt ferrites and synthesized nanocomposites. A decreasing trend with the increase in frequency was observed in dielectric loss as shown in Figure 10. This dependence upon frequency of dielectric loss is predicted by Koop's theory [39]. According to this theory, at low-frequency electrons move to the highly resistive grain boundaries results in high dielectric loss because more energy is required for the hopping mechanism between Fe^{+2} and Fe^{+3} ions following the applied electric field. Whereas electrons cannot move to the grain boundary due to the lagging behind of the applied electric field at high frequency, so minimum energy is needed for the electron hopping in low resistive grains region, thus the energy loss is minimum. Table 3 indicated an enormous increase in the dielectric loss with the increasing contents of MWCNTs. This is because of the formation of the voids and defects by the MWCNTs at the interfaces between MWCNTs and respective ferrite nanocomposites.

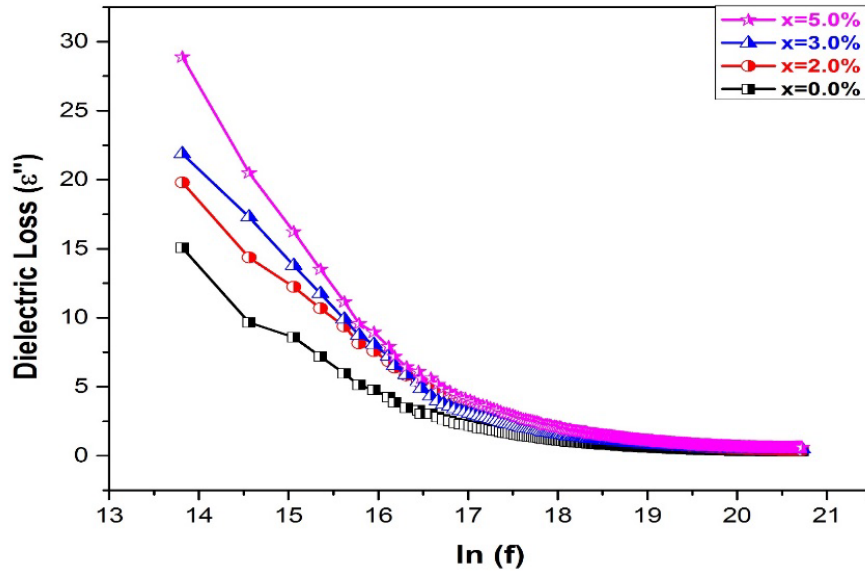


Figure 10: Variation of dielectric loss of pure CoFe_2O_4 and nanocomposites of $\text{CoFe}_2\text{O}_4/\text{MWCNTs}$ as a function of frequency and MWCNTs contents (wt. %).

3.4.3 Tangent Loss Factor

The ratio of the dielectric loss to the dielectric constant is known as tangent loss factor ($\tan \delta$) and is indicated variation upon the applied AC field as well as with MWCNTs content. It also indicates a similar decreasing behavior as observed in dielectric constant and dielectric loss with increasing frequency. Whereas increased tangent loss factor with increasing contents of MWCNTs is shown in Figure 11. This dependence upon frequency of tangent loss factor is in good agreement with Koop's theory as well as with Wagner-Maxwell model which was already discussed in detail in case of dielectric constant and loss. However, synthesized nanocomposites become suitable for high-frequency applications at such high-frequency

region due to the very small variation of $\tan \delta$ with frequency. In Table 2 an enormous increase in dielectric loss tangent was noticed in each sample with the increasing contents of MWCNTs due to the introduction of conducting networks in ferrites matrix.

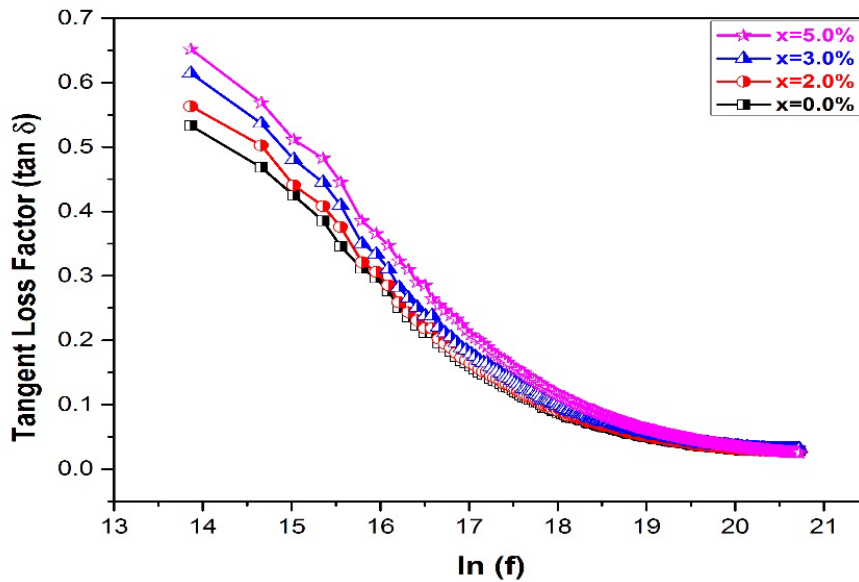


Figure 11: Tangent loss factor variation of pure CoFe_2O_4 and nanocomposites of $\text{CoFe}_2\text{O}_4/\text{MWCNTs}$ as a function of frequency and MWCNTs contents (wt. %).

3.4.4 AC Conductivity

The variation of synthesized pure cobalt ferrite and cobalt ferrite/MWCNTs nanocomposites with increasing frequency and increasing contents of MWCNTs is shown in Figure 12. The values of the alternating current (AC) conductivity at 1 MHz and 1GHz as well as at different concentrations of the MWCNTs are listed in Table 2. Generally, AC conductivity increases with increasing contents of MWCNTs. This is because of the MWCNT's domination resulting in band conduction domination in addition to hopping conduction due to their conductive nature. That's why pure cobalt ferrite has the lowest AC conductivity and nanocomposites with 5% MWCNTs have the highest value of AC conductivity. Also, the AC conductivity increases with increasing frequency because, in the low-frequency region, the grain boundaries are more active which are highly resistive. While in high-frequency regions, grains are more active which are conductive in nature.

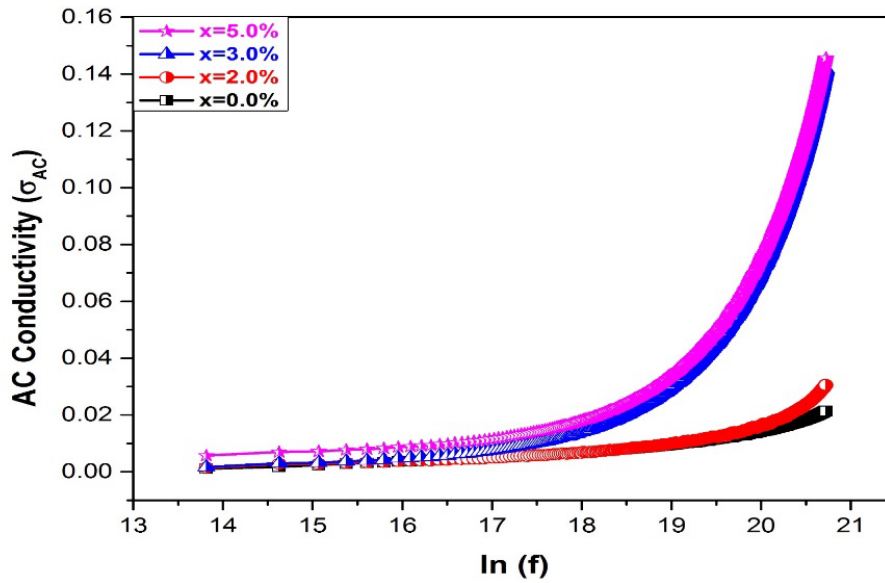


Figure 12: Variation of AC conductivity of pure CoFe_2O_4 and nanocomposites ($\text{CoFe}_2\text{O}_4/\text{MWCNTs}$) as a function of frequency and MWCNTs contents (wt. %).

4. Conclusion

In this work the chemical coprecipitation method was utilized effectively for the syntheses of cobalt ferrite nanoparticles. Ultrasonication technique with a polar dispersive medium like ortho-xylene was used in the nanocomposites of respective ferrite with MWCNTs contents (wt.%). The cubic spinel FFC phase of the synthesized ferrite was confirmed by the XRD patterns and in case of nanocomposites, no additional peaks in XRD patterns were observed confirming the efficiency of utilized method. Images obtained from SEM indicated effective coating MWCNTs with nanoparticles of cobalt ferrite and grain size obtained in all the samples that were in the range of 23-40 nm. FTIR Spectra confirmed the structural formation of the ferrite nanoparticles showing vibrational band ranges for tetrahedral and octahedral lattice sites. In all the samples, the dielectric properties and the AC conductivity were increased massively with the addition of the increasing content of MWCNTs. Whereas, with increasing frequency AC conductivity was increased and tangent loss factor, dielectric loss and dielectric constant were decreased. All these results indicated that for the improvement of dielectric properties, the MWCNTs are the best material with ferrites in the nanocomposites.

Acknowledgment

The authors would like to acknowledge the National University of Sciences and Technology (NUST), Islamabad for providing us funds for research work.

References

1. Yoon, T.J., et al., *Multifunctional nanoparticles possessing a "magnetic motor effect" for drug or gene delivery*. *Angewandte Chemie International Edition*, 2005. **44**(7): p. 1068-1071.
2. Simon, P. and Y. Gogotsi, *Materials for electrochemical capacitors*, in *Nanoscience And Technology: A Collection of Reviews from Nature Journals*. 2010, World Scientific. p. 320-329.
3. Murugesan, C., M. Perumal, and G. Chandrasekaran, *Structural, dielectric and magnetic properties of cobalt ferrite prepared using auto combustion and ceramic route*. *Physica B: Condensed Matter*, 2014. **448**: p. 53-56.
4. Kitamoto, Y., et al., *Co ferrite films with excellent perpendicular magnetic anisotropy and high coercivity deposited at low temperature*. *Journal of Applied physics*, 1999. **85**(8): p. 4708-4710.
5. Sousa, M.H., et al., *New electric double-layered magnetic fluids based on copper, nickel, and zinc ferrite nanostructures*. *The Journal of Physical Chemistry B*, 2001. **105**(6): p. 1168-1175.
6. Speliotis, D., *Magnetic recording beyond the first 100 years*. *Journal of Magnetism and Magnetic Materials*, 1999. **193**(1-3): p. 29-35.
7. Mazaleyrat, F. and L. Varga, *Ferromagnetic nanocomposites*. *Journal of Magnetism and Magnetic Materials*, 2000. **215**: p. 253-259.
8. Lee, J.-G., J.Y. Park, and C.S. Kim, *Growth of ultra-fine cobalt ferrite particles by a sol-gel method and their magnetic properties*. *Journal of Materials science*, 1998. **33**(15): p. 3965-3968.
9. Wu, H., et al., *Solvothermal synthesis of cobalt ferrite nanoparticles loaded on multiwalled carbon nanotubes for magnetic resonance imaging and drug delivery*. *Acta biomaterialia*, 2011. **7**(9): p. 3496-3504.
10. Routray, K.L., S. Saha, and D. Behera, *Effect of CNTs blending on the structural, dielectric and magnetic properties of nanosized cobalt ferrite*. *Materials Science and Engineering: B*, 2017. **226**: p. 199-205.
11. Nikumbh, A., et al., *Structural, electrical, magnetic and dielectric properties of rare-earth substituted cobalt ferrites nanoparticles synthesized by the co-precipitation method*. *Journal of Magnetism and Magnetic Materials*, 2014. **355**: p. 201-209.
12. Melo, R., et al., *Magnetic ferrites synthesised using the microwave-hydrothermal method*. *Journal of Magnetism and Magnetic Materials*, 2015. **381**: p. 109-115.
13. Liu, B.H., et al., *Microstructural evolution and its influence on the magnetic properties of CoFe₂O₄ powders during mechanical milling*. *Physical Review B*, 2006. **74**(18): p. 184427.
14. Xiao, S.H., et al., *Low-temperature auto-combustion synthesis and magnetic properties of cobalt ferrite nanopowder*. *Materials Chemistry and Physics*, 2007. **106**(1): p. 82-87.
15. Cannas, C., et al., *CoFe₂O₄ nanocrystalline powders prepared by citrate-gel methods: synthesis, structure and magnetic properties*. *Journal of Nanoparticle Research*, 2006. **8**(2): p. 255-267.
16. Moumen, N. and M. Pileni, *New syntheses of cobalt ferrite particles in the range 2– 5 nm: comparison of the magnetic properties of the nanosized particles in dispersed fluid or in powder form*. *Chemistry of materials*, 1996. **8**(5): p. 1128-1134.
17. Ahn, Y., et al., *Magnetization and Mössbauer study of cobalt ferrite particles from nanophase cobalt iron carbonate*. *Materials Letters*, 2001. **50**(1): p. 47-52.
18. Iijima, S., *Helical microtubules of graphitic carbon*. *nature*, 1991. **354**(6348): p. 56.
19. Treacy, M.J., T. Ebbesen, and J. Gibson, *Exceptionally high Young's modulus observed for individual carbon nanotubes*. *Nature*, 1996. **381**(6584): p. 678.
20. Wong, E.W., P.E. Sheehan, and C.M. Lieber, *Nanobeam mechanics: elasticity, strength, and toughness of nanorods and nanotubes*. *science*, 1997. **277**(5334): p. 1971-1975.

21. Ebbesen, T., et al., *Electrical conductivity of individual carbon nanotubes*. Nature, 1996. **382**(6586): p. 54.
22. Salam, M.A., M.A. Gabal, and A.Y. Obaid, *Preparation and characterization of magnetic multi-walled carbon nanotubes/ferrite nanocomposite and its application for the removal of aniline from aqueous solution*. Synthetic Metals, 2012. **161**(23-24): p. 2651-2658.
23. Özdemir, Z.G., et al., *Super-capacitive behavior of carbon nano tube doped 11-(4-cyanobiphenyl-4-oxy) undecan-1-ol*. Journal of Molecular Liquids, 2015. **211**: p. 442-447.
24. Ali, A.A., et al., *MWCNTs/carbon nano fibril composite papers for fuel cell and super capacitor applications*. Journal of Electrostatics, 2015. **73**: p. 12-18.
25. Kumar, R., et al., *Graphene-wrapped and cobalt oxide-intercalated hybrid for extremely durable super-capacitor with ultrahigh energy and power densities*. Carbon, 2014. **79**: p. 192-202.
26. Liu, Y., et al., *EMI shielding performance of nanocomposites with MWCNTs, nanosized Fe₃O₄ and Fe*. Composites Part B: Engineering, 2014. **63**: p. 34-40.
27. Tan, L., et al., *Removal of uranium (VI) ions from aqueous solution by magnetic cobalt ferrite/multiwalled carbon nanotubes composites*. Chemical Engineering Journal, 2015. **273**: p. 307-315.
28. Ghasemi, A., *The role of multi-walled carbon nanotubes on the magnetic and reflection loss characteristics of substituted strontium ferrite nanoparticles*. Journal of Magnetism and Magnetic Materials, 2013. **330**: p. 163-168.
29. Verma, A., A. Saxena, and D. Dube, *Microwave permittivity and permeability of ferrite-polymer thick films*. Journal of Magnetism and Magnetic Materials, 2003. **263**(1-2): p. 228-234.
30. Hussain, S.T., et al., *Decoration of carbon nanotubes with magnetic Ni_{1-x}CoxFe₂O₄ nanoparticles by microemulsion method*. Journal of Alloys and Compounds, 2012. **544**: p. 99-104.
31. Scherrer, P., *Determination of the size and internal structure of colloidal particles using X-rays*. Nachr. Ges. Wiss. Göttingen, 1918. **2**: p. 98-100.
32. Lehman, J.H., et al., *Evaluating the characteristics of multiwall carbon nanotubes*. Carbon, 2011. **49**(8): p. 2581-2602.
33. Soomro, S.A., et al., *Dielectric properties evaluation of NiFe₂O₄/MWCNTs nanohybrid for microwave applications prepared via novel one step synthesis*. Ceramics International, 2017. **43**(5): p. 4090-4095.
34. Waldron, R., *Infrared spectra of ferrites*. Physical review, 1955. **99**(6): p. 1727.
35. Zhang, Q., et al., *Synthesis and characterization of carbon nanotubes decorated with manganese-zinc ferrite nanospheres*. Materials Chemistry and Physics, 2009. **116**(2-3): p. 658-662.
36. Koops, C., *On the dispersion of resistivity and dielectric constant of some semiconductors at audiofrequencies*. Physical Review, 1951. **83**(1): p. 121.
37. Kumar, H., et al., *Dielectric behaviour of cobalt ferrite nanoparticles*. Int J Electr Electron Eng, 2013. **2**: p. 59-66.
38. Zhou, X.-B., et al., *Preparation of nanocrystalline-coated carbon nanotube/NiO. 5ZnO. 5Fe₂O₄ composite with excellent electromagnetic property as microwave absorber*. Journal of Physics D: Applied Physics, 2013. **46**(14): p. 145002.
39. George, M., et al., *Finite size effects on the electrical properties of sol-gel synthesized CoFe₂O₄ powders: deviation from Maxwell-Wagner theory and evidence of surface polarization effects*. Journal of Physics D: Applied Physics, 2007. **40**(6): p. 1593.